Inorganic Chemistry

ARTICLE

pubs.acs.org/IC

Investigation of Porous Ni-Based Metal−Organic Frameworks Containing Paddle-Wheel Type Inorganic Building Units via High-Throughput Methods

Palanikumar Maniam and Norbert Stock*

Institut für Anorganische Chemie, Christian-Albrechts-Universität zu Kiel, Max-Eyth-Strasse 2, D-24118 Kiel, Germany

Supporting Information

ABSTRACT: In the search of Ni based metal−organic frameworks (MOFs) containing paddle-wheel type building units, three chemical systems Ni^{2+}/H_nL/base/solvent with H_nL = H_3BTC (1,3,5-benzenetricarboxylic acid), H_3BTB (4,4′,4″,-benzene-1,3,5-triyl-tris-(benzoic acid)), and H_2BDC (terephthalic acid) were investigated using high-throughput (HT) methods. In addition to the conventional heating, for the first time HT microwave assisted synthesis of MOFs was carried out. Six new compounds were discovered, and their fields of formation were established. In the first system, H_3BTC was employed and a comprehensive HT-screening of compositional and process parameters was conducted. The synthesis condition for the Ni paddle-wheel unit was determined and two compounds $[Ni_3(BTC)_2(Me_2NH)_3]\cdot(DMF)_4(H_2O)_4$ (**1a**) and $[Ni_6(BTC)_2(DMF)_6(HCOO)_6]$ (**1b**) were discovered (Me_2NH = dimethylamine, DMF = dimethylformamide). In the second system, the use of the extended tritopic linker H_3BTB and the synthesis conditions for the paddle-wheel units led to the porous MOF, $[Ni_3(BTB)_2(2\text{-MeIm})_{1.5}(H_2O)_{1.5}]\cdot(DMF)_9(H_2O)_{6.5}$ (**2**), (2-MeIm = 2-methylimidazole). This compound shows a selective adsorption of H_2O and H_2 with a strong hysteresis. In the third system, H_2BDC was used, and the base (DABCO) was incorporated as a bridging ligand into all structures. Thus, two pillared layered porous MOFs $[Ni_2(BDC)_2(DABCO)]\cdot(DMF)_4(H_2O)_{1.5}$ (**3a**) and $[Ni_2(BDC)_2(DABCO)]\cdot(DMF)_4(H_2O)_4$ (**3b**) as well as a layered compound $[Ni(BDC)(DABCO)]\cdot(DMF)_{1.5}(H_2O)_2$ (**3c**) were isolated. The **3a** and **3b** polymorphs of the $[Ni_2(BDC)_2(DABCO)]$ framework can be selectively synthesized. The combination of microwave assisted heating, low overall concentration, stirring of the reaction mixtures, and an excess of DABCO yields a highly crystalline pure phase of **3b**. The fields of formation of all compounds were established, and scale-up was successfully performed for **1b**, **2**, **3a**, **3b**, and **3c**. All compounds were structurally characterized. In addition to IR, elemental and TG analyses, gas and vapor sorption experiments were carried out.

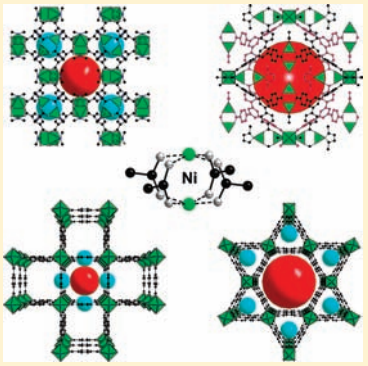

INTRODUCTION

High-throughput (HT) methodologies which are regarded as a core component in the screening of new drugs in the pharmaceutical field are also very helpful in the area of solid state chemistry.[1−3] By implementing this alternative method in solvothermal syntheses, many groups have discovered new compounds such as zeolites, metal-arsenates, -phosphonates, -carboxylates and -imidazolates.[4−8] In contrast to conventional methods, HT methods allow the rapid and systematic investigation of large synthesis fields.[3,9] This enables the efficient discovery of new compounds, the fast optimization of synthesis conditions, and because of the large amount of data, it allows the extraction of reaction trends. HT methods have been successfully applied in the investigation of porous metal−organic frameworks (MOFs), which are of interest because of their potential application in fields such as gas storage, gas separation, catalysis, and drug delivery.[10,11] Using HT methods, compounds such as MIL-101-NDC,[12] the amino-functionalized MOFs MIL-53, MIL-88, and MIL-101[13,14] and imidazolate based compounds such as ZIF-8 have been discovered.[8]

One of the most intensively investigated MOF to-date is HKUST-1 $[Cu_3(BTC)_2(H_2O)_3]$ which contains paddle-wheel type inorganic building units.[15] The chemical and thermal stability as well as the presence of accessible Lewis acid sites are some of the reasons why HKUST-1 has been studied by many groups. A search in the CSD database shows that most of the compounds containing paddle-wheel units are based on Cu and Zn, but examples with other ions such as Mo, Fe, and Cr were also reported.[16] Only few nickel carboxylates with paddle-wheel units have been described. While most of these nickel compounds exhibit no porosity,[17−20] only two porous structures were recently reported.[21,22] The combination of porosity and the presence of coordinatively unsaturated Ni^{2+} sites is also of special interest because of catalytic properties[23,24] and the strong H_2 binding affinity.[25,26] The accessibility of the metal sites in the these compounds depends very much on the nature and size of Ni-based inorganic units. Simple dimeric clusters such paddle-wheel units provide much less steric hindrance and thus, could enhance host−guest interactions. For these reasons, we started a systematic investigation to explore the feasibility of synthesizing

Received: February 23, 2011
Published: May 03, 2011

porous Ni^{2+} based MOFs with paddle-wheel units. Starting from the well established linkers 1,3,5-benzenetricarboxylic acid (H_3BTC), 4,4′,4″,-benzene-1,3,5-triyl-tris(benzoic acid) (H_3BTB) and terephthalic acid (H_2BDC), we investigated the three chemical systems Ni^{2+}/H_nL/base/solvent with H_nL = H_3BTC, H_3BTB, and H_2BDC. Here we report the fields of formation of six compounds, four containing Ni paddle-wheel units, in these three systems, and their structural elucidation, as well as their detailed characterization.

EXPERIMENTAL SECTION

Material and Methods. All reagents are of analytical grade (Sigma-Aldrich and ABCR) and were used without any further purification. H_3BTB was provided by BASF SE. High-throughput X-ray powder diffraction (XRPD) experiments were carried out in transmission mode using a STOE Stadi P combi high-throughput X-ray powder diffractometer equipped with an image-plate position-sensitive detector (IPPSD). MIR spectra were recorded with an ATI Matheson Genesis spectrometer in the spectral range 4000−400 cm^{-1} using the KBr disk method. Thermogravimetric analyses were carried out in air (75 mL min^{-1}, 30−800 °C, 4 °C min^{-1}) or nitrogen (75 mL min^{-1}, 30−800 °C, 4 °C min^{-1}) atmosphere using a NETZSCH STA 409 CD analyzer. CHN analyses were performed with a Eurovektor EuroEA Elemental Analyzer. The SEM images and semiquantitative elemental analyses were performed with a Phillips ESEM XL 30 and JEOL JSM-6500F hot cathode scanning electron microscope equipped with an energy dispersive X-ray (EDX) EDAX analyzer for elemental analysis. N_2, CO_2, Ar, and H_2O sorption experiments were performed using a Belsorp-max apparatus (BEL JAPAN INC.). Low pressure volumetric hydrogen sorption measurements were conducted with a Quantachrome Autosorb 1-C instrument at 77 K; H_2 as well as He gases of 99.999% purity were used. For the activation prior to sorption measurement, all samples were heated overnight at 150 °C in vacuum (10^{-3} mbar).

High-Throughput Experiments (Conventional Heating). The reaction system Ni^{2+}/H_nL/base/solvent was investigated using various molar ratios Ni^{2+}:H_nL:base (discovery and focused arrays) employing high-throughput methods. The process and compositional parameters are listed in the Supporting Information, Tables S1−S15. The HT experiments via conventional heating were performed under solvothermal conditions in a custom-made stainless steel high-throughput reactor system containing 48 PTFE inserts each with a maximum volume of 300 μL.[27] For most of the HT-experiments, standard solutions of starting materials were made by dissolving all solid reagents in the solvent under magnetic stirring (Supporting Information, Tables S1−S15). Respective volumes of each reactant were manually dosed into the PTFE inserts. In some of the HT-experiments, solid reactants with low solubility were weighed in directly into the Teflon inserts. The exact amounts of starting materials are given in the Supporting Information, Table S1−S15. The evaluations of the HT experiments are based on XRPD measurements.

High-Throughput Experiments (Microwave Heating). The system Ni^{2+}/H_2BDC/DABCO/DMF was investigated under microwave assisted heating. All reactions were performed using Anton Paar Synthos 3000 multimode microwave unit employing a 4 × 24MG5 rotor. Sealed borosilicate glass vials with reaction mixtures were used, which were inserted into the silicon carbide plate (6 × 4 matrix). The temperature of the plates is monitored using an IR sensor located at the bottom of the microwave unit. Samples requiring stirring were agitated with 10 mm magnetic stir bars during synthesis. The exact amounts of starting materials and reaction conditions are given in the Supporting Information, Tables S16−S19. The evaluations of the HT experiments are based on XRPD measurements.

$[Ni_3(BTC)_2(Me_2NH)_3]\cdot(DMF)_4(H_2O)_4$ (1a). In a HT experiment **1a** was obtained by the following procedure (molar ratio Ni-$(NO_3)_2\cdot6H_2O$/H_3BTC/2-MeIm = 2:1.5:1). DMF solutions of Ni-$(NO_3)_2\cdot6H_2O$ (0.03 mmol, 30 μL), H_3BTC (0.015 mmol, 60 μL), 2-MeIm (0.01 mmol, 10 μL), and DMF (100 μL) were pipetted into a 300 μL reactor. The mixture was heated at 170 °C for 48 h in a conventional oven. The synthesis of compound **1a** could not be scaled-up in glass reactors or larger Teflon reactors. Therefore, a larger amount of the pure phase product was collected from a separate HT experiment containing 24 identical reaction mixtures with the molar ratio $Ni(NO_3)_2\cdot6H_2O$/H_3BTC/2-MeIm = 2:1.5:1. The product (69 mg, 35% based on H_3BTC) containing dark green octahedral crystals (SEM micrograph Supporting Information, Figure S1) was washed with fresh DMF and identified by XRPD measurements. The measured and simulated XRPD patterns (Supporting Information, Figure S4) compare well. Elemental analysis of $[Ni_3(BTC)_2(Me_2NH)_3]\cdot(DMF)_4(H_2O)_4$ (**1a**), M = 1090.02 g mol^{-1}: found C 39.6, H 5.1, N 9.3; calcd C 39.6, H 5.8, N 9.0.

$[Ni_6(BTC)_2(HCOO)_6(DMF)_6]$ (1b). In a HT experiment, **1b** was obtained by the following procedure (molar ratio $Ni(ClO_4)_2\cdot6H_2O$/H_3BTC/2-MeIm = 3:1:1). DMF solutions of $Ni(ClO_4)_2\cdot6H_2O$ (0.03 mmol, 60 μL), H_3BTC (0.01 mmol, 40 μL), 2-MeIm (0.01 mmol, 20 μL), and DMF (80 μL) were pipetted into a 300 μL reactor. The mixture was heated at 150 °C for 48 h in a conventional oven. The scale-up of **1b** was accomplished in DURAN glass tubes with V_{max} = 4 mL by employing $Ni(ClO_4)_2\cdot6H_2O$ (0.3 mmol, 109.7 mg), H_3BTC (0.1 mmol, 21.0 mg), 2-MeIm (0.1 mmol, 8.2 mg) and 2 mL of DMF. The product (49.4 mg, 67% based on H_3BTC) containing green hexagonal plates (SEM micrograph Supporting Information, Figure S1) was washed with fresh DMF and identified by XRPD measurements. The measured and simulated XRPD patterns (Supporting Information, Figure S4) compare well. Elemental analysis of $[Ni_6(BTC)_2(HCOO)_6(DMF)_6]$ (**1b**), M = 1475.05 g mol^{-1}: found C 34.5, H 4.0, N 5.8; calcd C 34.2, H 3.7, N 5.7.

$[Ni_3(BTB)_2(2\text{-MeIm})_{1.5}(H_2O)_{1.5}]\cdot(DMF)_9(H_2O)_{6.5}$ (2). In a HT experiment under conventional heating **2** was obtained by the following procedure (molar ratio $Ni(NO_3)_2\cdot6H_2O$/H_3BTB/2-MeIm = 1.5:3:3.5). DMF solutions DMF of $Ni(NO_3)_2\cdot6H_2O$ (0.015 mmol, 15 μL), H_3BTB (0.03 mmol, 105 μL), 2-MeIm (0.035 mmol, 35 μL), and DMF (45 μL) were pipetted into a 300 μL reactor. The mixture was heated at 170 °C for 48 h. The scale-up of **2** was accomplished in a batch Teflon-lined steel autoclave with V_{max} = 20 mL by employing $Ni(NO_3)_2\cdot6H_2O$ (1.5 mmol, 436 mg), H_3BTB (3 mmol, 1314 mg), 2-MeIm (3.5 mmol, 287 mg), and 20 mL of DMF. The product (769 mg, 78% based on $Ni(NO_3)_2\cdot6H_2O$) containing dark brown blocks (SEM micrograph Supporting Information, Figure S1) was washed with fresh DMF and identified by XRPD measurements. The measured and simulated XRPD patterns (Supporting Information, Figure S5) compare well. Elemental analysis of $[Ni_3(BTB)_2(2\text{-MeIm})_{1.5}(H_2O)_{1.5}]\cdot(DMF)_9(H_2O)_{6.5}$ (**2**), M = 1971.83 g mol^{-1}: found C 52.6, H 5.4, N 8.8; calcd C 52.9, H 6.0, N 8.5.

$[Ni_2(BDC)_2(DABCO)]\cdot(DMF)_4(H_2O)_{1.5}$ (3a). In a HT experiment under conventional heating, **3a** was obtained by the following procedure (molar ratio $Ni(NO_3)_2\cdot6H_2O$/H_2BDC/DABCO = 2:2:1). DMF solutions of $Ni(NO_3)_2\cdot6H_2O$ (0.02 mmol, 20 μL), H_2BDC (0.02 mmol, 60 μL), DABCO (0.01 mmol, 10 μL), and DMF (110 μL) were pipetted into a 300 μL reactor. The mixture was heated at 110 °C for 48 h. The scale-up of **3a** was accomplished in a batch Teflon-lined steel autoclave with V_{max} = 20 mL by employing $Ni(NO_3)_2\cdot6H_2O$ (2 mmol, 580 mg), H_2BDC (2 mmol, 332 mg), DABCO (1 mmol, 112 mg) and 20 mL of DMF. The product (614 mg, 70% based on H_2BDC) containing green microcrystalline powder (SEM micrograph Supporting Information, Figure S1) was washed with fresh DMF and identified by XRPD measurements (Supporting Information, Figure S6). Elemental analysis of $[Ni_2(BDC)_2(DABCO)]\cdot(DMF)_4(H_2O)_{1.5}$ (**3a**), M = 877.12 g mol^{-1}: found C 46.2, H 5.4, N 9.3; calcd C 46.5, H 5.8, N 9.6.

dx.doi.org/10.1021/ic200381f |Inorg. Chem. 2011, 50, 5085–5097

Table 1. Crystallographic Data for $[Ni_3(BTC)_2(Me_2NH)_3]\cdot(DMF)_4(H_2O)_4$ (1a), $[Ni_6(BTC)_2(DMF)_6(HCOO)_6]$ (1b), and $[Ni_3(BTB)_2(2\text{-MeIm})_{1.5}(H_2O)_{1.5}]\cdot(DMF)_9(H_2O)_{6.5}$ (2)

	1a[a]	1b	2a[a]
chemical formula	$Ni_3C_{36}H_{63}N_7O_{20}$	$Ni_6C_{42}H_{54}N_6O_{30}$	$Ni_3C_{87}H_{118}N_{12}O_{29}$
formula weight (g/mol)	1090.02	1475.05	1971.83
crystal system	cubic	trigonal	cubic
space group	$Fm\bar{3}m$ (No. 225)	$P\bar{3}$ (No. 147)	$Im\bar{3}$ (No. 204)
a (Å)	26.5941(7)	13.8230(4)	26.816(3)
b (Å)	26.5941(7)	13.8230(4)	26.816(3)
c (Å)	26.5941(7)	7.9625(2)	26.816(3)
α (deg)	90	90	90
β (deg)	90	90	90
γ (deg)	90	120	90
V (Å^3)	18808.6(9)	1317.60(6)	19283(6)
Z	16	1	8
λ (Å)	0.71013	0.71013	0.71013
D_{calcd} (g cm^{-3})	1.025	1.859	0.831
μ (mm^{-1})	1.23	2.20	0.62
temp (K)	293	120	293
R1 (on F_o^2, $I > 2\sigma(I)$)	0.068	0.040	0.076
wR2 (on F_o^2, $I > 2\sigma(I)$)	0.180	0.070	0.239

[a] The SQUEEZE routine of the program PLATON was used to eliminate the contribution of disordered solvents molecules.[29]

$[Ni_2(BDC)_2(DABCO)]\cdot(DMF)_4(H_2O)_4$ (3b). In a HT-MW experiment **3b** was obtained by the following procedure (molar ratio $Ni(NO_3)_2\cdot6H_2O/H_2BDC/DABCO$ = 1:1:4). DMF solutions of $Ni(NO_3)_2\cdot6H_2O$ (0.1 mmol, 200 μL), H_2BDC (0.1 mmol, 300 μL), DABCO (0.4 mmol, 800 μL), and DMF (700 μL) were pipetted into a 4 mL glass vial. The mixture was heated under stirring in the microwave unit at 110 °C for 2 h (set power value =400 W). Larger amounts of **3b** were obtained by using a separate HT-MW experiment containing six identical reaction mixtures with the molar ratio $Ni(NO_3)_2\cdot6H_2O/H_2BDC/DABCO$ = 1:1:4. The product (163 mg, 59% based on H_2BDC) containing green microcrystalline powder (SEM micrograph Supporting Information, Figure S1) was washed with fresh DMF and identified by XRPD measurements (Supporting Information, Figure S6). Elemental analysis of $[Ni_2(BDC)_2(DABCO)]\cdot(DMF)_4(H_2O)_4$ (**3b**), M = 922.23 g mol^{-1}: found C 43.8, H 5.7, N 9.2; calcd C 44.3, H 6.1, N 9.1.

$[Ni(BDC)(DABCO)]\cdot(DMF)_{1.5}(H_2O)_2$ (3c). In a HT-MW experiment **3c** was obtained by the following procedure (molar ratio $Ni(NO_3)_2\cdot6H_2O/H_2BDC/DABCO$ = 3:1:4). DMF solutions of $Ni(NO_3)_2\cdot6H_2O$ (0.3 mmol, 600 μL), H_2BDC (0.1 mmol, 300 μL), DABCO (0.4 mmol, 800 μL), and DMF (300 μL) were pipetted into a 4 mL glass vial. The mixture was heated in the microwave unit at 110 °C for 2 h (set power value = 400 W). Larger amounts of **3c** were obtained using a separate HT-MW experiment containing six identical reaction mixtures with the molar ratio $Ni(NO_3)_2\cdot6H_2O/H_2BDC/DABCO$ = 3:1:4. The product (153 mg, 53% based on H_2BDC) containing pale green microcrystalline powder (SEM micrograph Supporting Information, Figure S1) was washed with fresh DMF and identified by XRPD measurements (Supporting Information, Figure S6). Elemental analysis of $[Ni(BDC)(DABCO)]\cdot(DMF)_{1.5}(H_2O)_2$ (**3c**), M = 480.65 g mol^{-1}: found C 46.2, H 6.0, N 10.4; calcd C 46.2, H 6.4, N 10.2.

X-ray Crystallography. Suitable crystals of the compounds were carefully selected from the HT experiments using a polarizing microscope. Single-crystal X-ray diffraction for **1a** and **2** were performed with a STOE IPDS-1 diffractometer equipped with a fine-focus sealed tube (Mo-Kα radiation, λ = 71.073 pm). For data reduction and absorption correction the programs XRED and XSHAPE were used.[28] For **1a** and **2**, contributions from disordered solvent molecules were removed by the SQUEEZE routine (PLATON).[29] The single crystal of **1b** was measured using a Bruker−Nonius APEX II CCD diffractometer equipped with a Bruker−Nonius FR591 rotating anode Mo-Kα radiation source. Absorption correction was done using the SADABS software.[30] The single crystal structures were solved by direct methods and refined using the program package SHELXTL.[31] The results of single crystal structure determinations are summarized in Table 1. The structure of compound **3c** was solved using the following software programs: EXPO2009,[32] Material Studio,[33] and FOX.[34] The full Rietveld refinement of compounds **3a**, **3b**, and **3c** were carried out with TOPAS.[35] Results and final Rietveld refinement plots are given in Table 2 and Supporting Information, Figures S7−S9. Comparison of Ni−O and Ni−N bond lengths of the paddle-wheel based Ni(II) compounds are summarized in the Supporting Information, Table S20.

RESULTS AND DISCUSSION

The systematic investigation of a chemical system comprises a large number of parameters. Many chemical parameters such as molar ratios of starting materials, the overall concentration, additives (e.g., a base), the solvent, or the metal salt employed have a strong influence on the product formation and the phase purity.[36,37] Furthermore, process parameters such as the heating program, the reaction time, and the reaction temperature have to be taken into account.[38] To identify the reaction conditions leading to Ni-based paddle-wheel units, all these parameters were investigated. Starting from so-called discovery arrays, large parts of the parameter fields are scanned. Once a new compound is discovered, focused arrays are set up which focus on a smaller part or the parameter space and thus allow us to establish the optimized synthesis conditions.[27] In the following sections the results of our HT- investigations of the three respective systems are described and discussed.

HT-Investigation of the System Ni^{2+}/H_3BTC/Base/Solvent. The first and most extensive screening of the reaction parameters was carried out in the first system Ni^{2+}/H_3BTC/base/solvent (Figure 1). At first the influence of different bases,

dx.doi.org/10.1021/ic200381f |Inorg. Chem. 2011, 50, 5085–5097

Table 2. Crystallographic Data for $[Ni_2(BDC)_2(DABCO)]\cdot(DMF)_4(H_2O)_{1.5}$ (3a), $[Ni_2(BDC)_2(DABCO)]\cdot(DMF)_4(H_2O)_4$ (3b), and $[Ni(BDC)(DABCO)]\cdot(DMF)_{1.5}(H_2O)_2$ (3c)

	3a	3b	3c
chemical formula	$Ni_2C_{34}H_{51}N_6O_{13.5}$	$Ni_2C_{34}H_{56}N_6O_{16}$	$NiC_{18.5}H_{30.5}N_{3.5}O_{7.5}$
formula weight (g/mol)	877.12, 557.75[a]	922.23, 557.75[a]	480.65, 334.98[a]
crystal system	tetragonal	trigonal	monoclinic
calculated density ($g\cdot cm^{-3}$)	1.360, 0.861[a]	1.215, 0.735[a]	1.762, 1.228[a]
space group	*I*4/*mcm* (No. 140)	$P\bar{3}m1$ (No. 164)	*P*2/*m* (No. 10)
a (Å)	15.1496(7)	21.5930(3)	10.6682(7)
b (Å)	15.1496(7)	21.5930(3)	7.0125(4)
c (Å)	18.6597(8)	9.3672(1)	6.0822(4)
α (deg)	90	90	90
β (deg)	90	90	95.269(5)
γ (deg)	90	120	90
V ($Å^3$)	4282.6(4)	3782.4(1)	453.1(1)
Z	4	3	1
λ (Å)	1.5406	1.5406	1.5406
2*θ* range (deg)	2.0 to 80.0	2.0 to 80.0	2.0 to 80.0
no. of non H-atoms	13	11	17
GoF	1.158	2.930	3.570
no. structural parameters	39	40	79
R_{wp}	0.044	0.054	0.139
R_p	0.033	0.039	0.097
R_{Bragg}	0.009	0.032	0.055

[a] The values are calculated without guest molecules.

imidazole (Im), 2-methylimidazole (2-MeIm), 1,4-diazabicyclo-[2.2.2]octane (DABCO), and 4,4-bipyridine (4,4-Bipy) in the system $NiCl_2\cdot6H_2O/H_3BTC$/base/DMF, was investigated varying the molar ratio Ni^{2+}/H_3BTC. At 150 °C, only 2-MeIm led to a new, well crystalline phase which was identified as $[Ni_3(BTC)_2(Me_2NH)_3]\cdot(DMF)_4(H_2O)_4$ (**1a**) and is isostructural to HKUST-1 (Supporting Information, Table S1).[15] In contrast to the copper-analogue HKUST-1 which can be obtained in various solvents without any additives via solvothermal, electrochemical, microwave, or sonothermal methods (Supporting Information, Table S21), the presence of the base 2-MeIm is essential for the formation of **1a**. The role of 2-MeIm can not be explained up to now. It is not a structure directing agent since no 2-MeIm could be found in the final product **1a**.

To find the optimal Ni^{2+} source for the synthesis, different salts, that is, $NiCl_2\cdot6H_2O$, $NiSO_4\cdot6H_2O$, $Ni(ClO_4)_2\cdot6H_2O$, $Ni(CH_3COO)_2\cdot4H_2O$, and $Ni(NO_3)_2\cdot6H_2O$, were screened in combination with H_3BTC, 2-MeIm, and DMF at a reaction temperature of 150 °C (Figure 1, Supporting Information, Table S2). On the basis of the results of the XRPD measurements, $NiSO_4\cdot6H_2O$ and $Ni(CH_3COO)_2\cdot4H_2O$ produce only X-ray amorphous products while $Ni(ClO_4)_2\cdot6H_2O$ led exclusively to the new dense compound $[Ni_6(BTC)_2(DMF)_6(HCOO)_6]$ (**1b**). $Ni(NO_3)_2\cdot6H_2O$ yields most often a mixture of both phases **1a** and **1b** depending on the molar ratio of the reactants (Supporting Information, Table S2). Although the use of $NiCl_2\cdot6H_2O$ resulted always in the formation of **1a**, EDX measurements showed the presence of large amounts of Cl^- ions in the as synthesized product (Ni/Cl = 1:4−5). Removal of the Cl^- ions was investigated but always led to the structural decomposition. Therefore, $Ni(NO_3)_2\cdot6H_2O$ was used for all further investigations.

The use of various solvents well-known for the synthesis of MOFs and mixtures thereof were screened for the synthesis optimization of **1a** (Figure 1, Supporting Information, Table S3). On the basis of the results of the XRPD measurements, only pure, dry DMF led to the most crystalline and pure phase product **1a**. Nevertheless, small amounts of H_2O introduced through the use of $Ni(NO_3)_2\cdot6H_2O$ lead to the partial hydrolysis of DMF and the formation of dimethylamine (Me_2NH) and formic acid. While formate ions can act as anionic ligands, dimethylamine can act as a monodentate ligand or in the protonated form as a counterion to balance the framework charge.[39,40] In **1a** and **1b** dimethylamine and formate ions are observed, respectively.

The reaction temperature also plays a crucial role in solvothermal syntheses, especially with respect to the crystallinity and the yield of the phase.[38,41] Therefore, the reaction system Ni^{2+}/H_3BTC/2-MeIm in DMF was investigated at five different temperatures between 140 and 180 °C using 48 different starting compositions, each (Figure 2, Supporting Information, Tables S4−S8). The products were analyzed per XRPD measurements, and the results are plotted in ternary crystallization diagrams (Figure 2). In addition to **1a** and **1b**, a new crystalline phase was detected (**1c**) at temperatures between 150 and 170 °C, which rapidly decomposed upon exposure to air. This phase is only found at the edge of the crystallization diagram in the area of high 2-MeIm and low Ni^{2+} concentrations. **1a** and **1c** crystallize as dark green octahedral and rod-shaped crystals, respectively, while **1b** forms light green hexagonal crystals (Supporting Information, Figure S1). Figure 2 shows that **1a** preferentially forms at temperatures of 160−180 °C, but only at 170 °C crystals with a well-defined shape (octahedral morphology) were obtained (Supporting Information, Figure S1). Pure phase **1a** with high crystallinity was observed at the molar ratio $Ni(NO_3)_2/H_3BTC$/2-MeIm = 2:1.5:1 at 170 °C. Large amounts of **1a** could only be obtained in our 48-er reactor system. Title compound **1b** is the

dx.doi.org/10.1021/ic200381f |*Inorg. Chem.* 2011, 50, 5085–5097

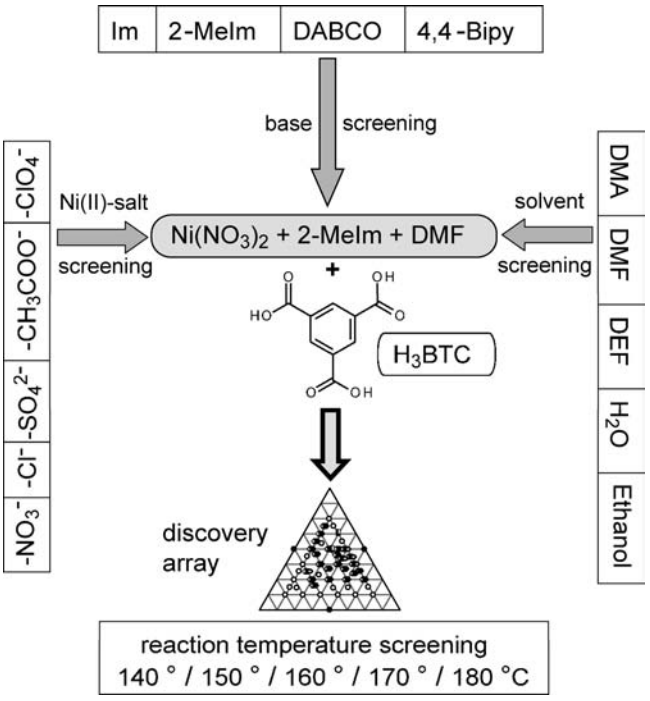

Figure 1. Summary of the HT screening of nickel(II) salts, bases, and solvents which provided the optimal reactants (shaded box) for the subsequent reaction temperature screening in HT-investigation of the system Ni^{2+}/H_3BTC/base/solvent. The definitions of the abbreviations used are following: Im = imidazole, 2-MeIm = 2-methylimidazole, DABCO = 1,4-diazabicyclo[2.2.2]octane, 4,4-Bipy =4,4-bipyridine, DMA = dimethylacetamide, DMF = dimethylformamide, DEF = diethylformamide, H_3BTC = 1,3,5-benzenetricarboxylic acid. Details of the experiments are given in Supporting Information, Tables S1−S3.

dominant phase at lower temperatures, and scale-up was easily accomplished.

HT-Investigation of $Ni(NO_3)_2/H_3BTB$/2-MeIm System. Once the synthesis condition of the Ni paddle-wheel unit for **1a** was established, H_3BTC was replaced with the extended linker H_3BTB and the optimal reactants and solvent, that is, nickel(II)-nitrate salt, 2-methylimidazole, and DMF, were employed. Using an initial reaction temperature of 150 °C and a reaction time of 72 h, a discovery array containing 48 different molar ratios of $Ni(NO_3)_2/H_3BTB$/2-MeIm were investigated. As shown in the crystallization diagram (Figure 3), only one crystalline phase is observed. Large dark brown cubic crystals of the paddle-wheel based structure $[Ni_3(BTB)_2(2\text{-MeIm})_{1.5}(H_2O)_{1.5}]\cdot(DMF)_9(H_2O)_{6.5}$ (**2**) were obtained (Supporting Information, Figure S2). Upon exposure to air the crystals change their color to green in minutes without the loss of crystallinity. The title compound is only formed in a small, well-defined area of the crystallization diagram (Figure 3). A focused array was set up to narrow down the compositional parameters, and the reaction temperature was varied between 130 and 170 °C. Well crystalline product of **2** is obtained at the molar ratio range $Ni(NO_3)_2/H_3BTC$/2-MeIm = 1.25−1.5:1.25−3.8:3−5.5 at 170 °C. Employing these conditions, the synthesis scale-up was carried out without any problems. In comparison to analogous Cu-based MOF-14 which is formed under mild synthesis conditions,[42] compound **2** prefers relatively high reaction temperatures and 2-methylimidazole as an additive.

HT-Investigation of Ni^{2+}/H_2BDC/DABCO System. Series of $[(M^{2+})_2(BDC)_2(DABCO)]$ (M = Ni, Co, Cu, Zn) paddle-wheel based porous MOFs with tetragonal framework structures were reported in recent years.[21,43−45] On the basis of the Cu-compound, Seki et al. proposed the structure model in 2001.[44] The tetragonal structure was later refined from single crystal XRD data of the isoreticular Zn-based compound.[45,46] A Zn-based polymorph of this MOF with a trigonal framework (Kagomé net topology[47]) was first synthesized by Chun et al. in a ternary solvent system.[48] The polymorph formation, tetragonal phase versus trigonal phase, can be controlled using different reaction times or using anion-templating as observed in mechanochemical synthesis.[49,50] While the Zn-based compounds have been studied in detail, almost no data is available on the Ni-based systems.[21,22] Rather than focusing only on the solvent system or the reaction time, we decided to study the polymorph formation by systematically investigating the compositional parameters as well as the reaction temperature. By employing the HT-reactor system, a discovery array was setup with 48 different $Ni(NO_3)_2/H_2BDC$/DABCO compositions using DMF as the sole solvent (Supporting Information, Figure S3 and Supporting Information, Tables S11−S14). Four temperatures (90°, 110°, 130°, and 150 °C) were chosen, and the reactors were subjected to conventional heating for 48 h. Both polymorphs, the tetragonal $[Ni_2(BDC)_2(DABCO)]\cdot(DMF)_4(H_2O)_{1.5}$ (**3a**) and trigonal $[Ni_2(BDC)_2(DABCO)]\cdot(DMF)_4(H_2O)_4$ (**3b**) phases were observed, and the new structure $[Ni(BDC)(DABCO)]\cdot(DMF)_{1.5}(H_2O)_2$ (**3c**) was discovered.

Title compound **3a** is the prevalent phase in the upper part of the crystallization diagram within the molar ratio range $Ni(NO_3)_2/H_2BDC$/DABCO = 1−5:2−6:1−4, whereas phase **3c** dominates the lower part in the molar ratio range $Ni(NO_3)_2/H_2BDC$/DABCO = 1−4:1:3−6. A scale-up synthesis of **3a** could be performed successfully using a 20 mL Teflon batch reactor with the optimal molar ratio $Ni(NO_3)_2/H_2BDC$/DABCO = 2:2:1 at 110 °C for 48 h. In the overlapping section of the **3a** and **3c** formation fields, title compound **3b** was observed. It always cocrystallizes as the minor phase with **3a** or **3c**. Comparing the number of occurrences of **3b** at different temperatures, this compound was predominantly formed at 110 °C (Supporting Information, Figure S3). Since in the corresponding Zn-based system, a short reaction time leads to the formation of the trigonal phase,[49] we also investigated the influence of the reaction time. A decrease to 1 h helps to increase the yield of **3b**, but the cocrystallization of **3a** could not be avoided (Figure 4, Supporting Information, Table S15). The results of HT-investigations via conventional heating at different reaction times have generally shown that both **3a** and **3b** are rapidly formed in relatively short time. In addition, only microcrystalline products of **3a** and **3b** have been obtained in all experiments. These factors indicate that the nucleation rate of both phases is high which usually leads to many small crystals.[51] To further investigate the polymorph formation, high-throughput experiments using microwave-assisted heating (HT-MW) with magnetic stirring were conducted (Figure 5). Microwave heating, which has been mostly utilized in the field of organic chemistry, is reported to have many advantages such as short reaction times, higher product yields, and increased product purity.[52,53] Recent reports have also shown that porous materials can be synthesized with microwave heating and most importantly, phase selectivity has been demonstrated, for example, for silicoaluminiumphosphates.[54,55] Therefore, the following studies were carried out: (a) influence of the molar ratios Ni^{2+}/H_2BDC/DABCO (Figure 5A), (b) role of stirring during the reaction (Figure 5B), (c) influence of the overall

dx.doi.org/10.1021/ic200381f |Inorg. Chem. 2011, 50, 5085–5097

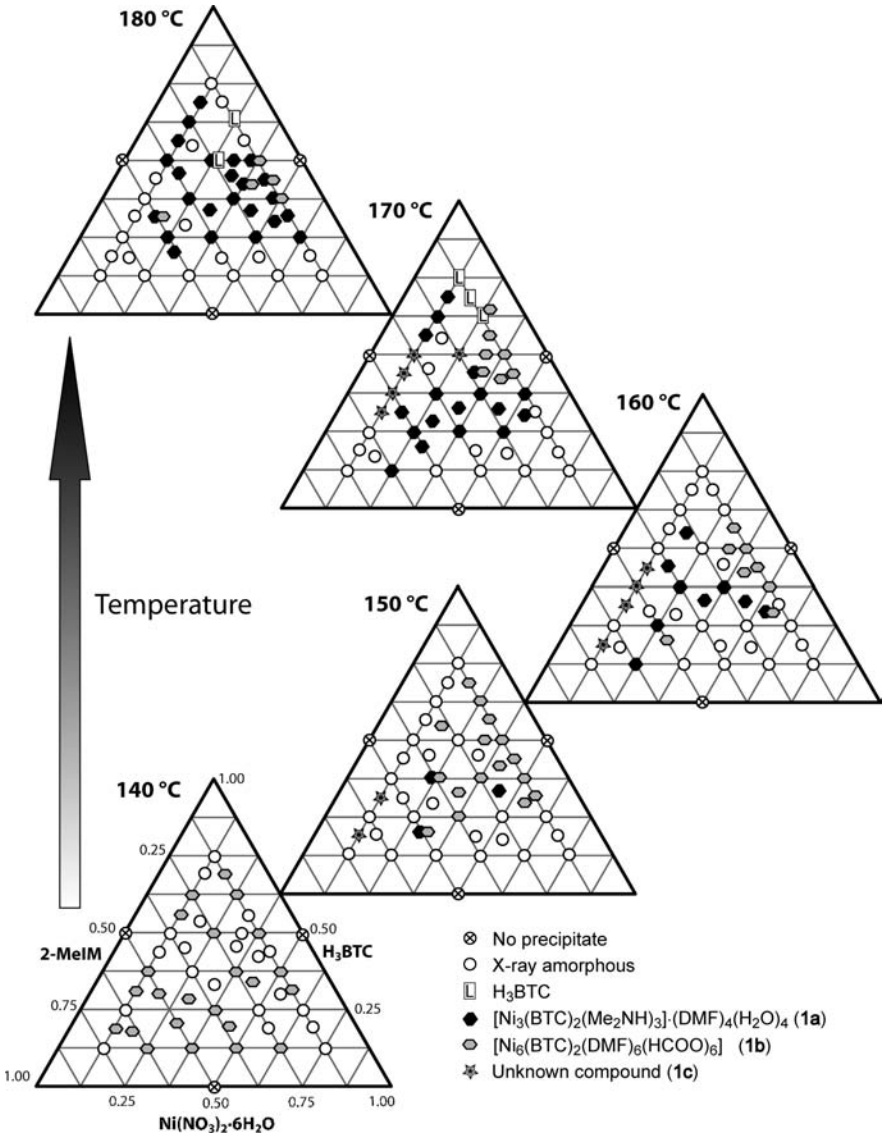

Figure 2. Ternary crystallization diagrams showing the results of HT reaction temperature screening between 140° and 180 °C. Compound **1b** dominates the formation fields at lower temperatures. **1a** forms preferentially at higher temperatures, mostly in the center of the diagram. **1c** crystallizes in a small formation field with high 2-MeIm amounts at 150−170 °C. Overlapping symbols stand for mixed phases. Results are based on XRPD measurements. Molar ratios of reactants are normalized to 1.00. Details of the experiments are given in Supporting Information, Tables S4−S8.

concentration (Figure 5C), and (d) influence of the Ni salt counterion (Figure 5D). These experiments were carried out repeatedly (2−3 times each) to confirm the trends observed.

On the basis of the previous results (Figure 4), molar ratios $Ni(NO_3)_2/H_2BDC$ = 1:1, 1.5:1, and 2:1 were chosen for the HT-MW experiment and the amount of DABCO was varied (Figure 5A, Supporting Information, Table S16). In contrast to the experiments under conventional heating (no stirring), pure phase **3b** could be obtained by applying the same reaction time and temperature. Employing a molar ratio of $Ni(NO_3)_2/H_2BDC/DABCO/DMF$ = 1:1:4:260 and microwave heating at 110 °C for 1 h under stirring yields a highly crystalline single-phase product of **3b**. Another HT-MW experiment was performed to cross-examine the stirring effect on the selective crystallization of **3a** and **3b** (Figure 5B, Supporting Information, Table S17). Interestingly, in this concentration regime pure phase of **3b** only forms under stirring and using large molar excess of DABCO, while the nonstirred reaction mixtures and smaller amounts of DABCO lead to the formation of **3a**. The effect of stirring on the phase selectivity is a relatively undeveloped field, and so far, it has been reported in the area of selective asymmetric synthesis[56,57] and synthesis of zeolites, for example, for zeolite Y polymorphs.[58]

The overall concentration has also a large influence on the product formation. In a HT-MW experiment, the $Ni(NO_3)_2/H_2BDC/x\cdot DABCO/y\cdot DMF$ (x = 0.5 and 4) reaction mixtures with y ranging from 65 to 5200 were investigated (Figure 5C, Supporting Information, Table S18, previously used concentrations in experiment 5B are marked by an asterisk). The results show that under highly diluted conditions and independent of stirring or base amount, only phase **3b** forms. Thus, the overall concentration exerts a greater influence on the product formation than the base amount. Under higher overall concentrations, the influence of stirring and base amount is observed. Phase **3a** crystallizes preferentially at concentrated conditions and low

dx.doi.org/10.1021/ic200381f |*Inorg. Chem.* 2011, 50, 5085–5097

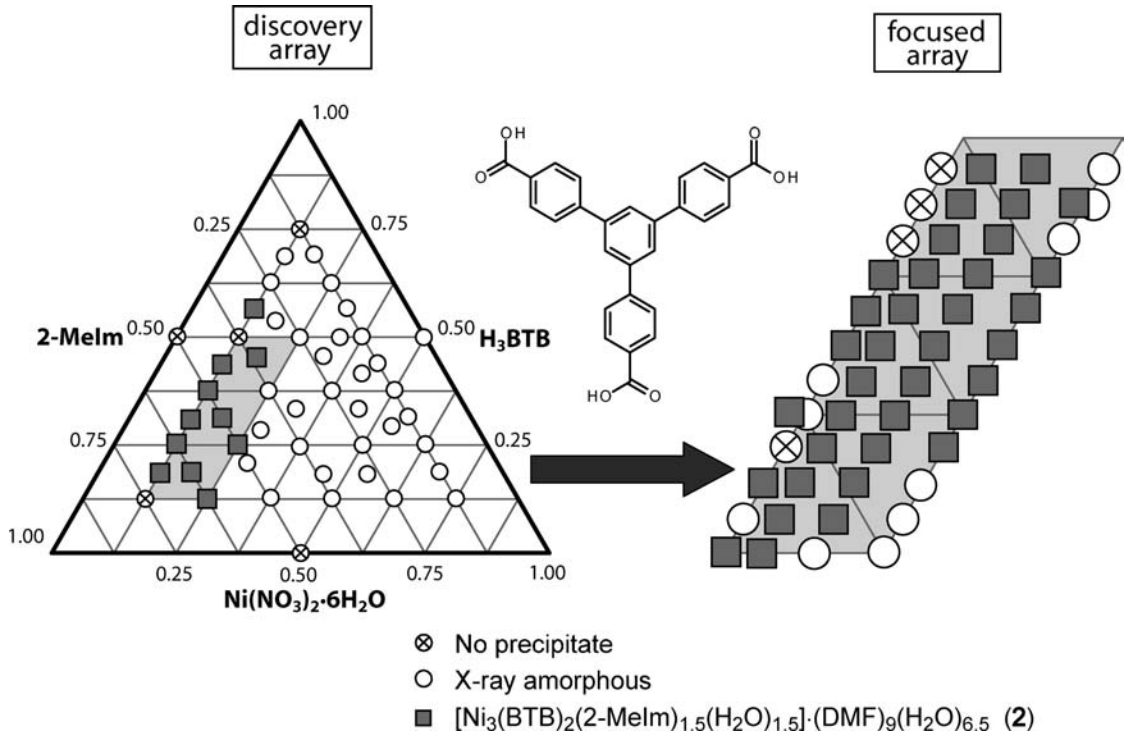

Figure 3. Crystallization diagram displaying the results of HT-investigations of the system $Ni^{2+}/H_3BTB/2\text{-MeIm/DMF}$. Reactions were conducted at 150 °C for 72 h in a conventional oven. Left: discovery array showing the approximate formation field of **2**. Right: focused array confirming the specific formation field of **2**. Results are based on XRPD measurements. Molar ratio values are normalized to 1.00. Details of the HT-experiment are given in Supporting Information, Tables S9−S10.

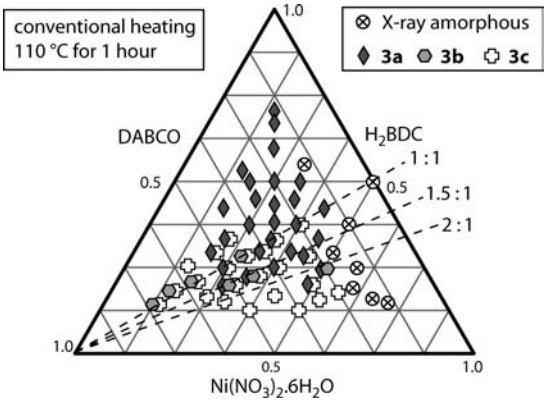

Figure 4. Crystallization diagram displaying the results of HT-investigations of the system $Ni(NO_3)_2/H_2BDC/DABCO$. Reactions were conducted at 110 °C for 1 h in a conventional oven. Formation of **3b** was observed at molar ratios $Ni(NO_3)_2/H_2BDC$ = 1:1, 1.5:1, and 2:1 (dashed lines). These parameters were used in the HT-MW setup for further investigations (Figure 5). Details of the HT-experiment are given in Supporting Information, Table S15.

amounts of base and phase **3c** forms exclusively at high overall concentration, an excess of DABCO and under stirring. Similar observations were also reported in the hydrothermal synthesis of Al/Cr-MIL-101 and Al/Cr-MIL-53, in which the former prefers dilute and more basic conditions whereas Al/Cr-MIL-53 requires concentrated and acidic conditions.[60,61] Recently Friscic et al. have demonstrated the anion-templating effect of nitrate and sulfate ions in the liquid assisted mechanochemical synthesis of the analogue Zn-based polymorphs.[50] Because of their synthesis procedure, the added anions were incorporated into the structure and lead to the phase selectivity. The addition of nitrate salts led to the formation of the tetragonal framework, while sulfate salts resulted in the formation of the trigonal framework structure. Therefore, we also investigated the role of NO_3^- and SO_4^{2-} anions of the Ni^{2+} salt on the product formation (Figure 5D, Supporting Information, Table S19). In the solvothermal HT-MW experiment, the NO_3^- salt leads to better crystalline products of **3a** and **3b**. Pure phase **3b** could not be obtained starting from the SO_4^{2-} salt. Thus the anion-templating effect cannot be transferred to the Ni-system with solvothermal reaction conditions.

Crystal Structure Description. The coordination of carboxylate ions to metal ions can be categorized in three types depending on the C−O···M angle.[62] Paddle-wheel units are defined as two M^{n+} ions which are bridged by four $(COO)^-$ ions in *syn-syn* mode (Figure 6). In this work, four porous nickel(II) based MOFs with paddle-wheel building units and two dense non paddle-wheel containing compounds were synthesized. Crystal structures of compounds **1a**, **1b**, and **2** were determined via single crystal X-ray diffraction, and Rietveld refinement was applied for the microcrystalline compounds **3a**, **3b**, and **3c**. Suitable starting structures were only available for **3a**, **3b**, and for **3c**, the structure solution was accomplished using in-house XRPD data.

*$[Ni_3(BTC)_2(Me_2NH)_3]\cdot(DMF)_4(H_2O)_4$ (**1a**).* Title compound **1a** has a 3D framework built of Ni(II) paddle-wheel units and tritopic BTC linker molecules. The paddle-wheel unit consists of four carboxylate fragments in the equatorial positions and two dimethylamine molecules in the axial positions (Figure 7,*i*). The axial ligands were formed in situ through the partial hydrolysis of

dx.doi.org/10.1021/ic200381f |*Inorg. Chem.* 2011, 50, 5085–5097

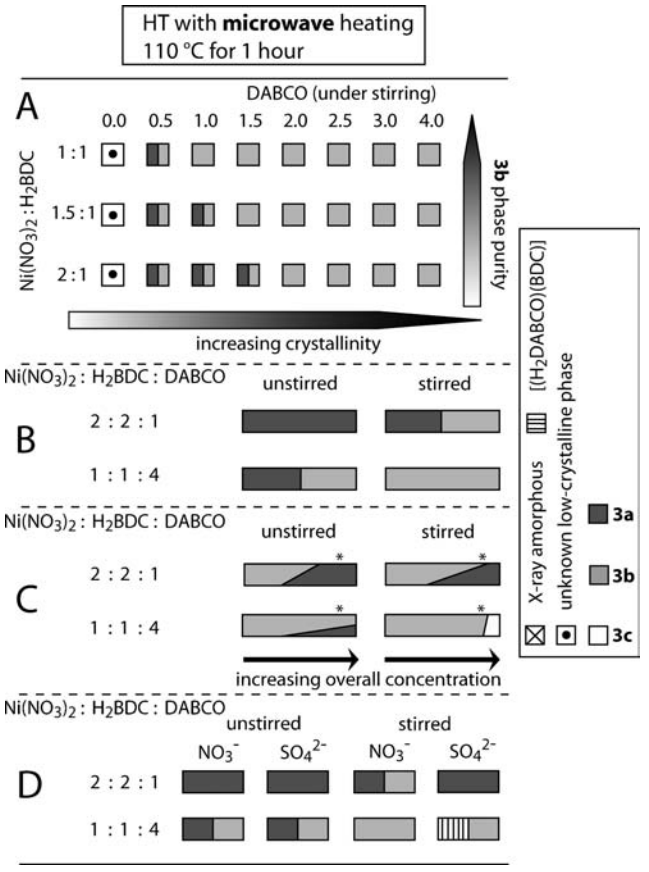

Figure 5. Results of HT-MW investigations of the system $Ni(NO_3)_2$/H_2BDC/DABCO/DMF. Under stirring, pure phase and highly crystalline **3b** was synthesized using large amounts of DABCO (**A**). In **B**, the effect of stirring on the product formation was studied with the optimal reactant molar ratios for **3a** (2:2:1:130) and **3b** (1:1:4:260). In **C**, the effect of the increasing overall concentration is shown for unstirred and stirred reaction mixtures, respectively [1 $Ni(NO_3)_2$/1 H_2BDC/x DABCO/y DMF, with x = 0.5, 4 and y = 65−5200]. The influence of sulfate and nitrate ions on the **3a**/**3b** formation is shown in diagram **D**. [$(H_2DABCO)(BDC)$] is the salt formed from protonated DABCO and benzenedicarboxylate ions.[59]

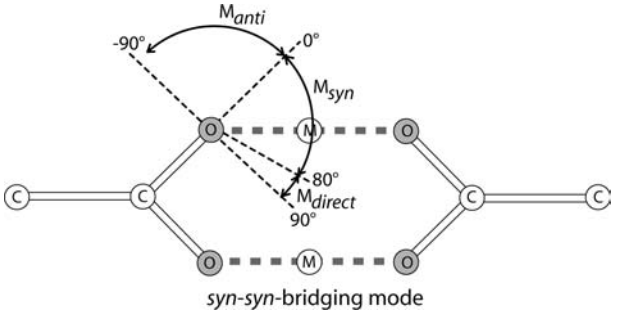

Figure 6. Three types of carboxylate ion coordination modes to metal ions. *Syn*-bonding: 0−80°, *direct* bonding: 80−90°, and *anti*-bonding: −90−0°. Thus, a paddle-wheel unit has a *syn-syn* bridging mode.[62]

DMF. Thus, each paddle-wheel unit contains two five-coordinated Ni^{2+} ions with distorted square pyramidal polyhedra. These units are connected to four carboxylate groups of the BTC linker to form a 3D (3,4)-connected **tbo-a**[63] framework

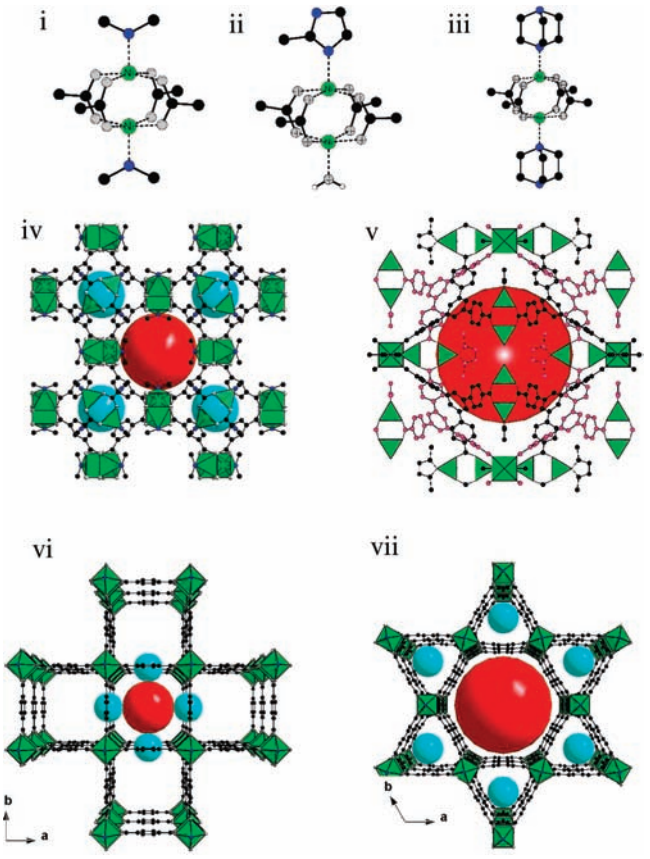

Figure 7. Paddle-wheel building units of (*i*) **1a** with two axial dimethylamine ligands, (*ii*) **2** with one axial water and one axial 2-methylimidazole ligand, (*iii*) **3a**/**3b** with two axial 1,4-diazabicyclo[2.2.2]octane ligands. Section of the crystal structures of **1a** (*iv*), view along [100], ∼9 and ∼5 Å pores, **2** with two interwoven nets (*v*), view along [100], 16 Å cavities, activated **3a** (*vi*), view along [001], 7 Å along *c* axis and 4 Å pores along the *a* and *b* axes, **3b** (*vii*), view along [001] 14 Å and 4 Å pores along the *c* axis and 3.5 Å pore windows along *a* and *b* axes. Square pyramidal NiO_5/NiO_4N units are displayed as green polyhedra.

with $Fm\bar{3}m$ symmetry. The structure of **1a** has two cages with inner pore diameters of ∼9 and ∼5 Å, respectively (Figure 7,*iv*). To the best of our knowledge, isostructural compounds have only been reported with copper, iron, molybdenum, and chromium.[15,64−66] The pores are occupied by DMF and H_2O molecules, which can be removed by thermal activation and renders the pores accessible to gas molecules.

$[Ni_3(BTB)_2(2\text{-}MeIm)_{1.5}(H_2O)_{1.5}]\cdot(DMF)_9(H_2O)_{6.5}$ (***2***). Compound **2** is built of Ni(II) paddle-wheel units which are composed of four carboxylate groups in equatorial positions and one water molecule as well as one 2-methylimidazole (2-MeIm) ligand in the axial positions. Similar to **1a**, the paddle-wheel units are connected to BTB linker molecules to construct an extended 3D (3,4)-connected **pto-a** network.[42,63] Because of freely rotating phenyl rings around the central phenyl ring of BTB linker (35° torsion angle), the symmetry of **2** is reduced to $Im\bar{3}$.[67] In analogy to the isostructural Cu(II)-based compound (MOF-14),[42] title compound **2** has a 2-fold interwoven network with a minimum displacement of 3 Å between the subframeworks (Figure 7,*v*). Although large cavities of approximately 16 Å are observed, the pore opening is restricted to a window of 3 × 4 Å (without the axial water ligands). The cavities are

occupied by DMF and water molecules. Upon thermal activation the guest molecules are removed. The crystallinity of sample increases drastically, and a structural transformation takes place (Supporting Information, Figure S5). The new reflections observed in the XRPD pattern of activated **2** can be explained by using a larger isomorphic unit cell (**2-ht**) and same space group $Im\bar{3}$ with cell parameters $3\cdot(a, b, c)$.[68]

$[Ni_2(BDC)_2(DABCO)]\cdot(DMF)_4(H_2O)_{1.5}$ (***3a***). Rietveld refinement of the compound **3a** was performed starting from the structure model of the isostructural Zn-based compound as it always crystallizes as a microcrystalline powder (Supporting Information, Figure S1, Table 2, Supporting Information, Figure S7).[45] As seen in Figure 7,*iii*, the paddle-wheel unit is comprised of four carboxylate groups and the DABCO ligands are located in the axial positions. A 2D layer with a (4,4) **sql**[63] grid is formed by the connection of the paddle-wheel units with BDC linkers in the *ab* plane. The layers are interconnected to form a pillared layered 3D structure via DABCO ligands along [001]. Two pore sizes of ~7 (along *c* axis) and ~4 Å (along *a* and *b* axes) are observed in the microporous structure of activated **3a** (Figure 7,*vi*). The as-synthesized compound crystallizes in the space group *I*4/*mcm* because of bent BDC linker molecules. Upon activation the symmetry changes to *P*4/*mmm* since the BDC linkers are now planar. This flexibility is caused by the presence and the type of guest molecules residing in the pores.[45]

$[Ni_2(BDC)_2(DABCO)]\cdot(DMF)_4(H_2O)_4$ (***3b***). Title compounds **3b** and **3a** exhibit polymorphic framework structures, containing different amounts of H_2O guest molecules. Rietveld refinement of the compound **3b** was performed starting from the structure model of the isostructural Zn-based compound as it always crystallizes as a microcrystalline powder (Supporting Information, Figure S1, Table 2, Supporting Information, Figure S8).[48] The structure consists of (3,4)-connected **kgm**[63] layers build by the paddle-wheel units and linked by the BDC molecules. These layers are interconnected by the DABCO molecules along the *c* axis, and a pillared 3D network is obtained. Along the *a* and *b* axes ~3.5 Å rectangular windows and along the *c* axis two types of pores with trigonal (4.5 Å) and hexagonal (14 Å) shapes are observed (Figure 7,*vii*). The pores are occupied by the DMF and water molecules. These can be removed by thermal activation, but under ambient conditions the structure decomposes gradually.

Whereas Zn^{2+} ions have a very flexible coordination environment, which can easily be distorted, Ni^{2+} ions exhibit preferentially quadratic planar and quadratic pyramidal coordination geometries. Because of the change from a (4,4) square grid in **3a** to a (3,4) Kagomé layer in **3b** (Supporting Information, Figure S10), ring strain is observed in the latter which could cause its structural instability. The information can also be used in the attempt to explain the formation of **3a** and **3b** under the different reaction conditions. Under conventional heating **3b** is preferentially formed at short reactions times, but we were never able to obtain a pure phase product. Only the use of microwave assisted heating as well as the optimal reaction conditions of low overall reaction mixture concentration, stirring, and excess base amounts led to single phase **3b**. By applying Ostwald's rule of stages,[69] the structure **3b** seems to be the kinetically preferred metastable product. This is also supported by the fact that **3b** has a lower framework density compared to **3a** ($\rho_{framework}$ = 0.735/0.861 g cm^{-3} for **3b** and **3a** respectively). Thus, during the product formation nucleation of **3b** should occur first. Under conventional heating, nuclei of both polymorphs are formed that grow to mixtures of **3a** and **3b**. Since crystals of **3a** are present, **3b** can undergo a solvent-mediated transformation to form the more thermodynamically stable **3a**.[70] Microwave assisted heating is known to increase the nucleation rate in crystallization processes.[71,72] Therefore, the results can be interpreted as follows: high solvent content together with stirring and large amounts of DABCO, microwave assisted heating leads exclusively to nuclei of **3b**. Because of the high nucleation rate, the reactant concentrations drop below the critical nucleation concentration necessary for the formation of **3a** and thereby, only crystals of **3b** are formed. Under these reaction conditions, a solvent mediated transformation is not observed since no crystal seeds of **3a** are present. These findings highlight the importance of microwave assisted heating compared to conventional methods in discovering new phases, investigating selective synthesis of polymorphs and less stable structures with larger pore sizes. In addition, this also supports the fact that the new metal−organic structures can be still obtained with well established common organic linkers such as terephthalic or trimesic acid by systematically trying out new synthesis methods. Often metastable products of a reaction system are overlooked because of inadequate understanding of the kinetic and thermodynamic parameters.

Crystal structure of non paddle-wheel based compounds (**1b**, **3c**): Compound $[Ni_6(BTC)_2(DMF)_6(HCOO)_6]$ (**1b**) crystallizes in a dense layered **kgd-a** structure with hexanuclear Ni_6O_{32} clusters similar to the isostructural Mn^{2+} compound.[39,63] Each Ni^{2+} ion is six-coordinated by oxygen atoms from one DMF molecule, three formate ions, and two BTC linkers to form distorted NiO_6 polyhedra. Six corner-sharing polyhedra form hexanuclear cores which are linked by BTC linkers to construct a 2D layered network along the *ab* plane (Supporting Information, Figure S11). The BTC linker molecules are all coordinated to the Ni ions in a *syn*-mode, while the sterically less hindered formate groups act as bridging ligands connecting three Ni^{2+} ions. Thus coordination in *syn*- and *anti*-mode is observed.

The structure of $[Ni(BDC)(DABCO)]\cdot(DMF)_{1.5}(H_2O)_2$ (**3c**) was solved from XRPD data. Title compound **3c** crystallizes in a layered (4,4) rectangular-grid topology containing NiO_4N_2 polyhedra.[73] Direct bonding of two carboxylate groups to the Ni^{2+} ion is observed (Figure 6), which leads to the formation of chains of alternating Ni^{2+} and BDC^{2-} ions along the *a* axis (Figure 8). These chains are connected along the *b* axis by the DABCO molecules to form layers. DMF and water molecules are located between these layers.

Sorption Measurements. Nitrogen sorption measurements were performed at 77 K on the title compounds with paddle-wheel building units (**1a**, **2**, **3a**, **3b**) to examine their porosity (Figure 9). The samples were first activated at 150 °C under vacuum for 12 h to remove the guest molecules in the pores. The experimental apparent specific surface area (Brunauer−Emmett−Teller (BET) method) and micropore volume of **1a** were determined to be 920 m^2/g and 0.35 cm^3/g respectively (Table 3). These values are smaller than expected probably because of partial decomposition of the structure or the incomplete activation. Different synthesis methods and improved activation procedures could yield higher porosity values. Isostructural copper-based HKUST-1 has been reported with surface areas and micropore volumes of 692−1820 m^2/g and 0.33−0.74 cm^3/g, respectively (Supporting Information, Table S21).

Compound **2** does not exhibit any porosity for nitrogen as anticipated because of the restricted pore window size of 3×4 Å (without the axial water ligands). On the other hand, the isostructural copper-based MOF-14 shows surface area of

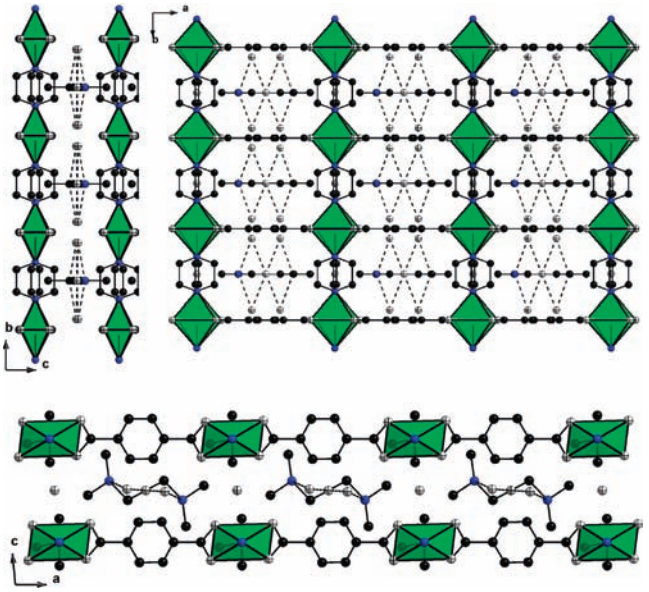

Figure 8. Sections of the crystal structure of the layered compound **3c**. Alternating BDC linkers and *direct*-bonded Ni^{2+} ions form chains along the *a* axis (bottom). Top left diagram showing DABCO molecules connecting the chains along the *b* axis. The hydrogen bonding (broken lines) between DMF and H_2O molecules are shown in the top right diagram in the *ab* plane.

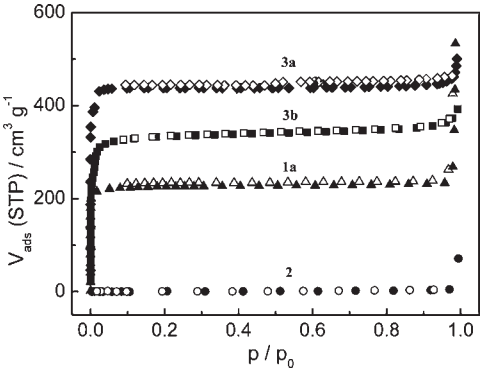

Figure 9. Nitrogen sorption isotherms measured at 77 K for the four paddle-wheel based Ni^{2+} compounds **1**, **2**, **3a**, and **3b**. All compounds with the exception of **2** exhibit microporous type I behavior. Solid symbols denote adsorption, hollow symbols denote desorption.

1502 m^2/g and a micropore volume of 0.53 cm^3/g (Supporting Information, Table S21).[42] Nevertheless, sorption experiments of **2** using other adsorbate molecules with smaller kinetic diameters[74] have shown increasing adsorption in the following order: $N_2 < Ar < H_2$ (77 K) and $CO_2 < H_2O$ (298 K) (Figure 10). Substantial hysteresis was observed in the H_2 and the H_2O sorption measurement. While for water as the adsorbent this is often observed, hysteresis in H_2 sorption measurements is rather rare. Interestingly, almost no H_2 molecules were liberated during the desorption process indicating a kinetic trapping of the adsorbates in the pores (Figure 10 inset graph).[75] The highest specific surface area was achieved with compound **3a**, and the experimental micropore volume is in good agreement with calculated values (Table 3, Figure 9). This proves the robustness and high stability of **3a**. In comparison to the lower micropore

Table 3. Specific Surface Areas and Micropore Volumes of the Paddle-Wheel Based Ni(II) Compounds[a]

		micropore volume/cm^3 g^{-1}	
compound	specific surface area S_{BET} (obs.)/m^2 g^{-1}	obs. at $p/p_0 = 0.5$	calcd (PLATON)[29]
1a	920	0.35	0.83
2	0	0	0.68
3a	1807	0.66	0.66
3b	1231	0.53	0.84

[a] Theoretical micropore volumes are calculated without the axial ligands.

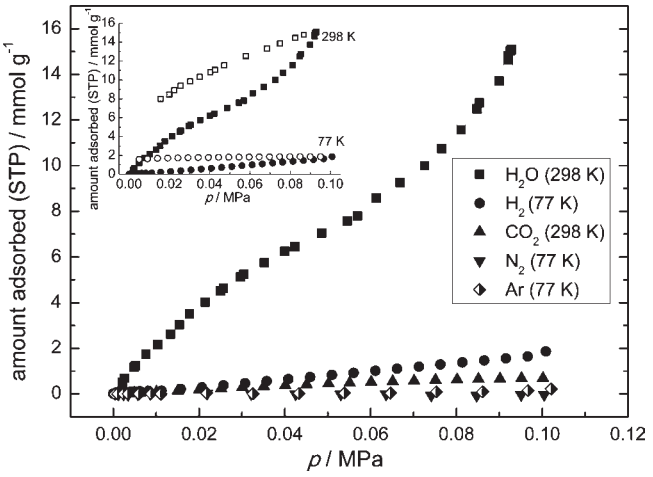

Figure 10. Increasing adsorption of molecules with decreasing kinetic diameters in compound **2**. Measurements using H_2, Ar, and N_2 were conducted at 77 K; H_2O and CO_2 at 298 K. The uptake depends strongly on the kinetic diameter of the guest molecules employed. The inset graph shows the hysteresis occurring during the desorption of H_2O and H_2 (solid symbols: adsorption, hollow: desorption).

volume of the polymorph **3b** with trigonal frameworks with the theoretical value indicates the decomposition of the structure which was confirmed via XRPD measurement. The comparison of values obtained with isostructural compounds with other transition metal ions are given in Supporting Information, Table S21.

Chemical and Thermal Stability. High thermal stability and inertness to air as well as moisture are some of the essential requirements for the application of porous MOFs. For these reasons, thermogravimetric (TG) analyses and XRPD measurements of samples exposed to air as well as solvent-exchanged samples were performed. The weight losses observed in the TG experiments deviate in some cases from the results of the elemental analyses. Slightly lower values in TG experiments are found since the content of the pores and cages can vary because of the gas flow at the beginning of the experiments. TG analysis of **1a** in nitrogen, $[Ni_3(BTC)_2(Me_2NH)_3]\cdot(DMF)_4(H_2O)_4$, revealed a gradual weight loss up to 320 °C which corresponds to the removal of four H_2O and three DMF molecules (obs. 26.9%, calcd 26.7%). The next significant weight loss up to 600 °C yielded elemental nickel (Supporting Information, Figure S12). The temperature-dependent XRPD measurements in a capillary (Supporting Information, Figure S12) confirm the

dx.doi.org/10.1021/ic200381f |*Inorg. Chem.* 2011, 50, 5085–5097

thermal stability of **1a** up to 300 °C. Upon exposure to ambient conditions **1a** decomposes rapidly at room temperature to form a green X-ray amorphous product (Supporting Information, Figure S2). Solvent-exchange experiments with diverse organic solvents such ethanol, dichloromethane, and acetonitrile have shown a rapid disintegration of the crystal structure which indicates the instability of compound **1a**. The TG curve of $[Ni_6(BTC)_2(HCOO)_6(DMF)_6]$ **1b** shows three weight losses. The first weight loss (14.5%, calcd 14.9%) up to 250 °C could be due to the loss of three coordinated DMF molecules. Between 250 and 350 °C a loss of 24.9% (calcd 24.0%) is observed which is in accordance with the removal of the other three coordinated DMF molecules and three formate ions (Supporting Information, Figure S12). The solid residue after the third weight loss was determined to be NiO.

Compound **2**, $[Ni_3(BTB)_2(2\text{-MeIm})_{1.5}(H_2O)_{1.5}]\cdot(DMF)_9(H_2O)_{6.5}$, with the BTB linker is stable in air after the thermal activation, and its crystallinity even increases (Supporting Information, Figure S5). Unlike compound **1a**, the crystal structure of **2** remains intact even after 72 h of stirring in pure dichloromethane at room temperature. Upon heating during TG analysis, compound **2** loses a considerable amount of guest molecules until the first plateau at 300 °C is reached (Supporting Information, Figure S12). The observed weight loss of 33.4% corresponds to eight H_2O and seven DMF molecules (calcd 33.2%). Above 350 °C the organic units decompose and NiO is formed. The XRPD measurement of the sample treated at 250 °C confirms the stability of the framework and the structural transformation to the isomorphic subgroup with an enlarged unit cell of $3\cdot(a, b, c)$.

During the thermal decomposition of **3a**, $[Ni_2(BDC)_2(DABCO)]\cdot(DMF)_4(H_2O)_{1.5}$ (Supporting Information, Figure S12), all guest molecules are liberated from the pores up to 290 °C in a two step process (obs. 36.6%, calcd 36.4%). The substantial weight loss from 290 to 800 °C can be attributed to the decomposition of two BDC and one DABCO linker molecules (obs. 48.6%, calcd 50.2%). The residual powder was determined to be NiO by XRPD. Compound **3a** is also stable against moisture since after treatment with water, the crystallinity was preserved. **3a** has also been found to be tolerant against solvents such as ethanol, dichloromethane, and acetonitrile in solvent exchange experiments at room temperature. TG analysis of the compound **3b**, $[Ni_2(BDC)_2(DABCO)]\cdot(DMF)_4(H_2O)_4$, which has a polymorphic framework, two weight loss steps because of the removal of the guest molecules are observed (Supporting Information, Figure S12). The first weight loss between 40−120 °C corresponds to the removal of four H_2O molecules (obs. 7.4%, calcd 7.8%), while the second weight loss (120−300 °C) can be attributed to the removal of the four DMF molecules (obs. 29.6%, calcd 31.7%). Further heating up to 800 °C led to NiO. Unlike **3a**, **3b** with the trigonal framework is moisture sensitive and gradual decomposition upon storage at ambient conditions is observed. This gradual decomposition of the **3b** crystal structure was also observed after solvent exchange experiments. The TG analysis of **3c**, $[Ni(BDC)(DABCO)]\cdot(DMF)_{1.5}(H_2O)_2$, shows that the guest molecules are removed in two steps up to 350 °C (obs. 29.2%, calcd 30.3%). Above 350 °C the oxidation of the organic linker molecules takes place, and NiO is formed.

IR Spectroscopy. All compounds were characterized by IR spectroscopy (Supporting Information, Figure S13, S14). Their IR spectra exhibit broad bands in the region between 3600 and 3100 cm^{-1}, which are due to ν(O−H) vibrations of the uncoordinated water molecules involved in weak hydrogen bonds. Weak aliphatic ν(C−H) bands are observed in the 2950−2850 cm^{-1}. For all compounds the aromatic C−H stretching bands could not be seen because of overlap with the broad O−H bands. Two sharp aromatic γ(C−H) bands of 1,3,5-BTC linker are observed at 770 ± 5 cm^{-1} and 725 ± 5 cm^{-1} in **1a**, and **1b**.[76] Three sharp aromatic γ(C−H) deformation bands of BTB linker of **2** were seen at 857, 783, and 705 cm^{-1}.[77] For compounds **3a**, **3b**, and **3c**, the bands observed at 810 ± 5 cm^{-1} and 750 ± 5 cm^{-1} are characteristic and correspond to the γ(C−H) and the δ(C−C) vibration of the 1,4-BDC linker, respectively.[78] The bands at 1090 ± 5 and 1055 ± 5 cm^{-1} could be due to the ν_{as}(C−N) and ν_s(C−N) vibrations of DABCO.[79] In all spectra, strong bands at 1670−1600 cm^{-1} and 1400−1350 cm^{-1} are observed which can be assigned to the ν_{as}(C−O) and ν_s(C−O) vibrations of the $-COO^-$ groups. Around 1680 cm^{-1} the band of the ν(C═O) vibration of DMF molecules is detected.

CONCLUSION

With the aid of high-throughput (HT) methods we have identified the fields of formation of six new compounds. In addition to four porous Ni based MOFs with paddle-wheel building units, two compounds with dense layered structures (**1b**, **3c**) were also discovered. All compounds were fully characterized. In the system containing H_3BTC as starting material, a comprehensive screening of compositional and process parameters allowed to establish the reaction conditions for the Ni paddle-wheel unit. Application of these reaction conditions and replacing H_3BTC with the extended tritopic linker molecule H_3BTB, the paddle-wheel containing compound **2** was discovered. Changing the tritopic to a ditopic linker molecule (H_2BDC) and adding DABCO as the base, the formation of two pillared layered structures with the composition $[Ni_2(BDC)_2(DABCO)]$ was accomplished. The synthesis condition for each polymorph was scrutinized by employing HT-methods under conventional and microwave assisted heating. Rapid nucleation via microwave assisted heating coupled with the systematic investigation has been proven valuable for selectively obtaining the MOF **3b**. On the basis of the results of this study, the synthesis of other Ni containing MOFs with paddle-wheel units should be feasible, which have been described previously mainly with Cu^{2+} and Zn^{2+} ions.

ASSOCIATED CONTENT

Supporting Information. Exact amounts used for the high-throughput synthesis, SEM and optical images, Rietveld refinement results, XRPD patterns, TGA analyses and IR spectra are available. This material is available free of charge via the Internet at http://pubs.acs.org. The Cambridge Crystallographic Data Center (CCDC) 802889−802894 contains the supplementary crystallographic data for this paper. These data can be obtained free of charge via the Internet at ww.ccdc.cam.ac.uk/conts/retrieving.html (or from the CCDC, 12 Union Road, Cambridge CB2 1EZ, U.K; fax, +44 1223 36033; e-mail, deposit@ccdc.ac.uk).

AUTHOR INFORMATION

Corresponding Author

*E-mail: stock@ac.uni-kiel.de. Phone: (+49)431-880-1675. Fax: (+49)431-880-1775.

■ ACKNOWLEDGMENT

The authors thank Inke Jess (Christian-Albrechts-Universität zu Kiel) and Dr. Alexandra Lieb (Otto-von-Guericke-Universität Magdeburg) for the acquisition of single crystal data, Adam Wutkowski (Christian-Albrechts-Universität zu Kiel) for TG measurements, Steffen Schmidt (Ludwig-Maximilians-Universität München) for high-resolution SEM images, Prof. Michael Fröba, Ute Sazama, and Sandra Maracke (Universität Hamburg) for H_2-sorption measurements. The work has been supported by the State of Schleswig-Holstein and the Deutsche Forschungsgemeinschaft (DFG) through the priority program SPP 1362 "Porous Metal−Organic Frameworks" under Grant STO 643/5-1.

■ REFERENCES

(1) Koinuma, H.; Takeuchi, I. *Nat. Mater.* **2004**, *3*, 429–438.
(2) Maier, W. F.; Stöwe, K.; Sieg, S. *Angew. Chem., Int. Ed.* **2007**, *46*, 6016. *Angew. Chem.* **2007**, *119*, 6122–6179.
(3) Stock, N. *Microporous Mesoporous Mater.* **2010**, *129*, 287–295.
(4) Stock, N.; Bein, T. *Solid State Sci.* **2003**, *5*, 1207–1210.
(5) Akporiaye, D. E.; Dahl, I. M.; Karlsson, A.; Wendelbo, R. *Angew. Chem., Int. Ed.* **1998**, *37*, 609–611. *Angew. Chem.* **1998**, *110*, 629–631.
(6) Stock, N.; Bein, T. *Angew. Chem., Int. Ed.* **2004**, *43*, 749–752. *Angew. Chem.* **2004**, *116*, 767–770.
(7) Forster, P. M.; Burbank, A. R.; O'Sullivan, M. C.; Guillou, N.; Livage, C.; Férey, G.; Stock, N.; Cheetham, A. K. *Solid State Sci.* **2005**, *7*, 1549–1555.
(8) Banerjee, R.; Phan, A.; Wang, B.; Knobler, C.; Furukawa, H.; O'Keeffe, M.; Yaghi, O. M. *Science* **2008**, *319*, 939–943.
(9) Bauer, S.; Stock, N. *Chem. Unserer Zeit* **2007**, *41*, 390–398.
(10) Mueller, U.; Schubert, M.; Teich, F.; Puetter, H.; Schierle-Arndt, K.; Pastré, J. *J. Mater. Chem.* **2006**, *16*, 626–636.
(11) Horcajada, P.; Serre, C.; Vallet-Regi, M.; Sebban, M.; Taulelle, F.; Férey, G. *Angew. Chem., Int. Ed.* **2006**, *45*, 5974–5978. *Angew. Chem.* **2006**, *118*, 6120–6124.
(12) Sonnauer, A.; Hoffmann, F.; Fröba, M.; Kienle, L.; Duppel, V.; Thommes, M.; Serre, C.; Férey, G.; Stock, N. *Angew. Chem., Int. Ed.* **2009**, *48*, 3791–3794. *Angew. Chem.* **2009**, *121*, 3849–3852.
(13) Bauer, S.; Serre, C.; Devic, T.; Horcajada, P.; Marrot, J.; Férey, G.; Stock, N. *Inorg. Chem.* **2008**, *47*, 7568–7576.
(14) Ahnfeldt, T.; Gunzelmann, D.; Loiseau, T.; Hirsemann, D.; Senker, J.; Ferey, G.; Stock, N. *Inorg. Chem.* **2009**, *48*, 3057–3064.
(15) Chui, S. S.-Y.; Lo, S. M.-F.; Charmant, J. P. H.; Guy Orpen, A.; Williams, I. D. *Science* **1999**, *283*, 1148–1150.
(16) Allen, F. H. *Acta Crystallogr.* **2002**, *B58*, 380−388. Databank search in CSD Conquest version 5.31 with Feb 2010 update.
(17) Lee, S. W.; Kim, H. J.; Lee, Y. K.; Park, K.; Son, J.-H.; Kwon, Y.-U. *Inorg. Chim. Acta* **2003**, *353*, 151–158.
(18) Yuen, T.; Danilovic, D.; Li, K.; Li, J. *J. Appl. Phys.* **2008**, *103*, 07B725.
(19) Shi, Q.; Sun, Y.; Sheng, L.; Ma, K.; Cai, X.; Liu, D. *Inorg. Chim. Acta* **2009**, *362*, 4167–4173.
(20) Zhu, L.; Chen, X.; Zhao, Q.; Li, Z.; Zhang, X.; Sun, B. *Z. Anorg. Allg. Chem.* **2010**, *636*, 1441–1443.
(21) Arstad, B.; Fjellvåg, H.; Kongshaug, K. O.; Swang, O.; Blom, R. *Adsorption* **2008**, *14*, 755–762.
(22) Klein, N.; Herzog, C.; Sabo, M.; Senkovska, I.; Getzschmann, J.; Paasch, S.; Lohe, M. R.; Brunner, E.; Kaskel, S. *Phys. Chem. Chem. Phys.* **2010**, *12*, 11778–11784.
(23) Guillou, N.; Gao, Q.; Forster, P. M.; Chang, J.-S.; Noguès, M.; Park, S.-E.; Fèrey, G.; Cheetham, A. K. *Angew. Chem., Int. Ed.* **2001**, *40*, 2831–2834. *Angew. Chem.* **2001**, *113*, 2913–2916.
(24) Zou, R.-Q.; Sakurai, H.; Xu, Q. *Angew. Chem., Int. Ed.* **2006**, *45*, 2542–2546. *Angew. Chem.* **2006**, *118*, 2604–2608.
(25) Forster, P. M.; Eckert, J.; Heiken, B. D.; Parise, J. B.; Yoon, J. W.; Jhung, S. H.; Chang, J.-S.; Cheetham, A. K. *J. Am. Chem. Soc.* **2006**, *128*, 16846–16850.
(26) Lamberti, C.; Zecchina, A.; Groppo, E.; Bordiga, S. *Chem. Soc. Rev.* **2010**, *39*, 4951–5001.
(27) Maniam, P.; Näther, C.; Stock, N. *Eur. J. Inorg. Chem.* **2010**, 3866–3874.
(28) *XRED version 1.19, XSHAPE version 1.06*; Stoe & Cie GmbH: Darmstadt, Germany, 1999.
(29) Spek, A. L. *PLATON; a multipurpose crystallographic tool*; Utrecht University: Utrecht, The Netherlands, 2001.
(30) Sheldrick, G. M. *SADABS version*; Bruker AXS Inc., Madison, WI, 2007.
(31) Sheldrick, G. M. *Acta Crystallogr.* **2008**, *A64*, 112–122.
(32) Altomare, A.; Camalli, M.; Cuocci, C.; Giacovazzo, C.; Moliterni, A.; Rizzi, R. *J. Appl. Crystallogr.* **2009**, *42*, 1197–1202.
(33) *Materials Studio*, v5.0; Accelrys Software Inc.: San Diego, CA, 2009.
(34) Favre-Nicolin, V.; Cerny, R. *J. Appl. Crystallogr.* **2002**, *35*, 734–743.
(35) Coelho, A. A. *TOPAS-Academic; Program for indexing, structure resolution and Rietveld refinement on powder data*, V4.1; Bruker AXS Inc., Madison, WI, 2007.
(36) Bauer, S.; Bein, T.; Stock, N. *Inorg. Chem.* **2005**, *44*, 5882–5889.
(37) Biemmi, E.; Christian, S.; Stock, N.; Bein, T. *Microporous Mesoporous Mater.* **2009**, *117*, 111–117.
(38) Sonnauer, A.; Stock, N. *Eur. J. Inorg. Chem.* **2008**, 5038–5045.
(39) Chen, J.; Ohba, M.; Kitagawa, S. *Chem. Lett.* **2006**, *35*, 526–527.
(40) Biemmi, E.; Bein, T.; Stock, N. *Solid State Sci.* **2006**, *8*, 363–370.
(41) Forster, P. M.; Burbank, A. R.; Livage, C.; Férey, G.; Cheetham, A. K. *Chem. Commun.* **2004**, 368–369.
(42) Chen, B.; Eddaoudi, M.; Hyde, S. T.; O'Keeffe, M.; Yaghi, O. M. *Science* **2001**, *291*, 1021–1023.
(43) Takei, T.; Ii, T.; Kawashima, J.; Ohmura, T.; Ichikawa, M.; Hosoe, M.; Shinya, Y.; Kanoya, I.; Mori, W. *Chem. Lett.* **2007**, *36*, 1136–1137.
(44) Seki, K.; Takamizawa, S.; Mori, W. *Chem. Lett.* **2001**, *30*, 332–333.
(45) Dybtsev, D. N.; Chun, H.; Kim, K. *Angew. Chem., Int. Ed.* **2004**, *43*, 5033–5036. *Angew. Chem.* **2004**, *116*, 5143–5146.
(46) Chun, H.; Dybtsev, D. N.; Kim, H.; Kim, K. *Chem.—Eur. J.* **2005**, *11*, 3521–3529.
(47) Syozi, I. *Prog. Theor. Phys.* **1951**, *6*, 306–308.
(48) Chun, H.; Moon, J. *Inorg. Chem.* **2007**, *46*, 4371–4373.
(49) Kondo, M.; Takashima, Y.; Seo, J.; Kitagawa, S.; Furukawa, S. *CrystEngComm* **2010**, *12*, 2350–2353.
(50) Friscic, T.; Reid, D. G.; Halasz, I.; Stein, R. S.; Dinnebier, R. E.; Duer, M. J. *Angew. Chem., Int. Ed.* **2010**, *49*, 712–715. *Angew. Chem.* **2010**, *122*, 724–727.
(51) Dunitz, J. D.; Bernstein, J. *Acc. Chem. Res.* **1995**, *28*, 193–200.
(52) Herrero, M. A.; Kremsner, J. M.; Kappe, C. O. *J. Org. Chem.* **2008**, *73*, 36–47.
(53) Sonnauer, A.; Stock, N. *J. Solid State Chem.* **2008**, *181*, 3065–3070.
(54) Jhung, S. H.; Chang, J.-S.; Hwang, J. S.; Park, S.-E. *Microporous Mesoporous Mater.* **2003**, *64*, 33–39.
(55) Jhung, S. H.; Lee, J. H.; Forster, P. M.; Férey, G.; Cheetham, A. K.; Chang, J.-S. *Chem.—Eur. J.* **2006**, *12*, 7899–7905.
(56) Kondepudi, D. K.; Kaufman, R. J.; Singh, N. *Science* **1990**, *250*, 975–976.
(57) Mcbride, J. M.; Carter, R. L. *Angew. Chem., Int. Ed. Engl.* **1991**, *30*, 293–295. *Angew. Chem.* **1991**, *103*, 298–300.
(58) Hanif, N.; Anderson, M. W.; Alfredsson, V.; Terasaki, O. *Phys. Chem. Chem. Phys.* **2000**, *2*, 3349–3357.
(59) Yang, E.; Song, X.-C.; Zhu, J.-W. *Acta Crystallogr., Sect. E* **2008**, *64*, o1764.
(60) Ahnfeldt, T.; Guillou, N.; Gunzelmann, D.; Margiolaki, I.; Loiseau, T.; Fèrey, G.; Senker, J.; Stock, N. *Angew. Chem., Int. Ed.* **2009**, *48*, 5163–5166. *Angew. Chem.* **2009**, *121*, 5265–5268.
(61) Khan, N. A.; Jun, J. W.; Jhung, S. H. *Eur. J. Inorg. Chem.* **2010**, 1043–1048.

(62) Carrell, C. J.; Carrell, H. L.; Erlebacher, J.; Glusker, J. P. *J. Am. Chem. Soc.* **1988**, *110*, 8651–8656.
(63) O'Keeffe, M.; Peskov, M. A.; Ramsden, S. J.; Yaghi, O. M. *Acc. Chem. Res.* **2008**, *41*, 1782–1789.
(64) Xie, L.; Liu, S.; Gao, C.; Cao, R.; Cao, J.; Sun, C.; Su, Z. *Inorg. Chem.* **2007**, *46*, 7782–7788.
(65) Kramer, M.; Schwarz, U.; Kaskel, S. *J. Mater. Chem.* **2006**, *16*, 2245–2248.
(66) Murray, L. J.; Dinca, M.; Yano, J.; Chavan, S.; Bordiga, S.; Brown, C. M.; Long, J. R. *J. Am. Chem. Soc.* **2010**, *132*, 7856–7857.
(67) Ma, S.; Sun, D.; Ambrogio, M.; Fillinger, J. A.; Parkin, S.; Zhou, H.-C. *J. Am. Chem. Soc.* **2007**, *129*, 1858–1859.
(68) Wondratschek, H.; Müller, U. *International Tables for Crystallography*; Kluwer Academic Publishers: Dordrecht, The Netherlands, 2006, Vol. A1, p 689.
(69) Ostwald, W. *Z. Phys. Chem.* **1897**, *22*, 289–330.
(70) Davey, R. J.; Blagden, N.; Potts, G. D.; Docherty, R. *J. Am. Chem. Soc.* **1997**, *119*, 1767–1772.
(71) Gharibeh, M.; Tompsett, G. A.; Conner, W. C.; Yngvesson, K. S. *ChemPhysChem* **2008**, *9*, 2580–2591.
(72) Khan, N. A.; Haque, E.; Hwa Jhung, S. *Phys. Chem. Chem. Phys.* **2010**, *12*, 2625–2631.
(73) Natarajan, S.; Mahata, P. *Chem. Soc. Rev.* **2009**, *38*, 2304–2318.
(74) Li, J.-R.; Kuppler, R. J.; Zhou, H.-C. *Chem. Soc. Rev.* **2009**, *38*, 1477–1504.
(75) Zhao, X.; Xiao, B.; Fletcher, A. J.; Thomas, K. M.; Bradshaw, D.; Rosseinsky, M. J. *Science* **2004**, *306*, 1012–1015.
(76) Green, J. H. S.; Harrison, D. J.; Kynaston, W. *Spectrochim. Acta, Part A* **1971**, *27*, 793–806.
(77) Jutand, A.; Negri, S. *Eur. J. Inorg. Chem.* **1998**, *9*, 1811–1821.
(78) Arenas, J. F.; Marcos, J. I. *Spectrochim. Acta, Part A* **1980**, *36*, 1075–1081.
(79) McDivitt, J. R.; Humphrey, G. L. *Spectrochim. Acta, Part A* **1974**, *30*, 1021–1033.